Matsumoto, H., et al., 2021, Long-term Aptian marine osmium isotopic record of Ontong Java Nui activity: Geology, v. 49, https://doi.org/10.1130/G48863.1

Supplementary information on "Aptian marine osmium isotopic record of the Ontong Java Nui event"

Hironao Matsumoto[1*], Rodolfo Coccioni[2], Fabrizio Frontalini[3], Kotaro Shirai[1], Luigi Jovane[4], Ricardo Trindade[5], Jairo F. Savian[6], Maria Luisa G. Tejada[7], Silvia Gardin[8], Junichiro Kuroda[1]

[1]*Atmosphere and Ocean Research Institute, Japan, The University of Tokyo, 5-1-5 Kashiwanoha, Kashiwa 277-8564, Japan*

[2]*University of Urbino, Carlo Bo, 61029 Urbino, Italy*

[3]*DiSPeA, University of Urbino Carlo Bo, Italy, Campus Scientifico Enrico Mattei, Località Crocicchia, 61029 Urbino, Italy*

[4]*Instituto Oceanográfico, Universidade de São Paulo, Praça do Oceanográfico, 191 - São Paulo, SP 05508-120, Brazil*

[5]*Instituto de Astronomia, Geofísica e Ciências Atmosféricas, Universidade de São Paulo, Rua do Matão, 1226 - São Paulo, SP 05508-090, Brazil*

[6] *Departamento de Geologia, Instituto de Geociências, Universidade Federal do Rio Grande do Sul, Avenida Bento Gonçalves, 9500 – Porto Alegre, RS 91501-970, Brazil*

[7]*Institute for Marine Geodynamics, Japan Agency for Marine-Earth Science and Technology, 2-15, Natsushima-cho, Yokosuka-city, Kanagawa, 237-0061, Japan*

[8]*Centre de Rechereche en Paléontologie-Paris, UMR 7207, Sorbonne Universit é-MNHN-CNRS, 4, Place Jussieu, 75005, Paris, France*

MATERIALS AND METHODS

The sedimentary rock samples for Os and C isotopic analyses were collected from the Poggio le Guaine (PLG) section and the PLG core drilled nearby, located on the Monte Nerone ridge of the Umbria–Marche Basin in central Italy (Coccioni et al., 2012; Figs. 1 and DR1). The Upper Barremian to lowermost Aptian interval belongs to the Maiolica Formation and consists of white limestone with cyclic intercalation of black shale layers (Fig. 2) (Coccioni et al., 2012; Savian et al., 2016). The ~2 m-thick organic-rich Selli Level, which is the regional expression of OAE1a, occurs at the base of the Marne a Fucoidi Formation (0 m in Fig. 2: Coccioni et al., 1987; Coccioni, 2020). Above the Selli Level, the main lithologies of Lower to mid-Aptian stage are greenish-gray mud/marlstone, reddish marlstone, and minor siliceous sediments. A 20 cm-thick black shale horizon occurs ~1 m above the Selli Level and a 6 cm-thick black shale horizon occurs ~10 m above the Selli Level (Fig. 2). The lithology of the PLG core is comparable to that of nearby outcrops, namely the PLG (Coccioni et al., 2014) and Gorgo a Cerbara sections (Coccioni et al., 1987). We correlated the three sedimentary records with biostratigraphy, chemostratigraphy (Os and $\delta^{13}C_{carb}$), and lithological features. The sedimentary rock samples were collected from just above the Selli Level to ~11 m above it in the PLG core (Coccioni et al., 2012). Sedimentary rock samples were also collected

from the lowermost part of the PLG section that overlaps with the uppermost parts of the studied interval in the PLG core (Matsumoto et al., 2020). Since the black shales at ~3 and ~12 m of the composite depth scale were fractured during the drilling activity, these were not used for Os and C isotopic analyses. Instead, marlstone samples from just above and below the black shale horizons were used.

Cleaned samples were dried and powdered in an agate mill. After spiking, Re and Os in the hydrogenous fraction of the carbonate rocks were extracted using inverse aqua regia digestion. Abundances and isotopic compositions of Os were determined by negative thermal ionization-mass spectrometry (TRITON, Thermo Fisher Scientific, USA) at the Japan Agency for Marine-Earth Science and Technology (JAMSTEC, Japan). The Re abundances were determined by a quadrupole inductively coupled plasma-mass spectrometer (iCAP Qc, Thermo Fisher Scientific, USA) at JAMSTEC. The average procedural blanks of Os was 0.5±0.3 pg and $^{187}Os/^{188}Os$ was 0.11±0.03. The average Re procedural blank was 4±2 pg. Initial $^{187}Os/^{188}Os$ values (Os_i) were calculated from the measured $^{187}Os/^{188}Os$ and $^{187}Re/^{188}Os$ values, the age-depth model of the sediments (Table DR1), and the ^{187}Re decay constant (1.666×10^{-11} yr^{-1}; Smoliar et al., 1996). Detailed analytical methods for Os isotopic analysis were as described by Matsumoto et al. (2020). A marlstone sample at 4.1 m showed an extremely whitish color and had an anomalous

high Os_i (~1.35) value. Since this samples could have experienced different diagenesis or alternation compared to other samples, it was considered to be an outlier and discarded thereof (Fig. DR3, Table DR1).

The stable carbon isotope ratio of carbonate ($\delta^{13}C_{carb}$) was determined using isotope ratio-mass spectrometry (Delta V plus, Thermo Fisher Scientific, USA), equipped with an automated carbonate reaction device (GasBench II, Thermo Fisher Scientific, USA), at the Atmosphere and Ocean Research Institute, University of Tokyo (Japan). All isotope values are reported using delta notation with respect to PeeDee Belemnite (PDB), based on an NBS-19 value of −2.20‰ for $\delta^{18}O$ and+1.95‰ for $\delta^{13}C$. External reproducibility was estimated from the repeated analysis of the NBS-19 standard within an analysis batch and the typical values are better than 0.05‰ and 0.08% for $\delta^{18}O$ and $\delta^{13}C$, respectively (1 SD) (Table DR2). Detailed analytical conditions are reported in Shirai et al. (2018).

WEZEL LEVEL

The black shale horizon located around 3 m of the composite depth scale falls in the Ap7 carbon isotopic segment and the upper part of the *Leupoldina cabri* planktonic foraminiferal Zone. At the present state of knowledge, a similar and coeval horizon is

recorded in the Piobbico and Cismon cores (Tornaghi et al., 1989; Erba et al., 1999) and Gargano Promontory (Luciani et al., 2001) in Italy, but on the basis of the available stratigraphic data, it could also be recognized in the Vocontian Basin (Kößler et al. 2001; Herrle et al., 2004; Heimhofer et al., 2006), in southern Spain (De Gea et al., 2003; Quijano et al., 2012: Aguado et al., 2014), in northeastern Tunisia (Elkhazri et al., 2013) and in central Turkey (Hu et al., 2012). It is here proposed to name this undescribed black-shale horizon as "Wezel Level".

BOX MODEL CLACULATION

Changes in the Os flux through hydrothermal activities were calculated using a simple box model based on Tejada et al. (2009). This model assumes that the ocean is a unique Os reservoir, and marine Os content and $^{187}Os/^{188}Os$ reflect the balance between continental input, hydrothermal input related to oceanic crustal production and hydrothermal input associated with the OJN emplacement, extraterrestrial input, and a sedimentary sink. These relationships are described as:

$$\frac{dM_{ocean}}{dt} = F_{cont} + F_{hydr} + F_{cosm} + F_{OJN} - F_{sed} \quad (1)$$

$$\frac{d(M_{ocean}R_{ocean})}{dt} = F_{cont}R_{cont} + F_{hydr}R_{hydr} + F_{cosm}R_{cosm} + F_{OJN}R_{OJN} - F_{sed}R_{sed} \quad (2)$$

where M, F, and R indicate the amount, flux, and isotopic ratio of Os ($^{187}Os/^{188}Os$), and the subscripts 'ocean', 'cont', 'hydr', 'cosm', 'OJN', and 'sed' represent the oceanic reservoir, continental input, hydrothermal input, extraterrestrial input, input from the OJN, and sedimentary output, respectively. Indeed, we assumed that R_{sed} coincides with R_{ocean}. The above equations can be combined as:

$$\frac{dR_{ocean}}{dt} = \frac{[F_{cont}(R_{cont} - R_{ocean}) + F_{hydr}(R_{hydr} - R_{ocean}) + F_{OJN}(R_{OJN} - R_{ocean}) + F_{cosm}(R_{cosm} - R_{ocean})]}{M_{ocean}} \quad (3)$$

We adopted the present-day F_{cont}=295 t/kyr, R_{cont}=1.54 (Levasseur et al., 1999; Peucker-Ehrenbrink and Jahn, 2001); R_{hydr}=0.126 (Allegre and Luck, 1980), F_{cosm} =17.6 t/kyr, R_{cosm} = 0.126 (Levasseur et al., 1999; Allegre and Luck, 1980), and M_{ocean}=13,000t (Levasseur et al., 1998) for the steady background conditions before OAE1a. Also, we used F_{hydr}=414 t/kyr, F_{sed}=0.056×M_{ocean}, and R_{OJN}=0.146 based on Tejada et al. (2009).

We calculated the changes in the Sr flux through hydrothermal activities using a simple box model after Blättler et al. (2011). Like the box modeling of Os, relationship of Sr flux can be described as:

$$\frac{dM_{ocean}}{dt} = F_{cont} + F_{hydr} + F_{diag} + F_{OJN} - F_{sed} \quad (4)$$

$$\frac{d(M_{ocean}R_{ocean})}{dt} = F_{cont}R_{cont} + F_{hydr}R_{hydr} + F_{diag}R_{diag} + F_{OJN}R_{OJN} - F_{sed}R_{sed} \quad (5)$$

$$\frac{dR_{ocean}}{dt} = \frac{[F_{cont}(R_{cont} - R_{ocean}) + F_{hydr}(R_{hydr} - R_{ocean}) + F_{OJN}(R_{OJN} - R_{ocean}) + F_{diag}(R_{diag} - R_{ocean})]}{M_{ocean}} \quad (6)$$

where M, F, and R indicate the amount, flux, and isotopic ratio of Sr ($^{87}Sr/^{86}Sr$), and the subscripts 'ocean', 'cont', 'hydr', 'diag', 'OJN', and 'sed' represent the oceanic reservoir, continental input, hydrothermal input, diagenetic input, input from the OJN, and sedimentary output, respectively. We used $M_{ocean}=1.05\times10^{13}$ t, R_{cont},=0.7115, R_{hydr},=0.7033, R_{diag},=0.7084, $F_{cont}=1.59\times10^{9}$ t/kyr, $F_{hydro}=1.62\times10^{9}$ t/kyr, $F_{diag}=0.30\times10^{9}$ t/kyr (Palmer and Edmond, 1989; Blättler et al., 2011). In addition, we set R_{sed} and F_{sed} as $R_{sed}=R_{ocean}$ and $F_{sed}=M_{ocean}\times3.33\times10^{-4}$ t/kyr.

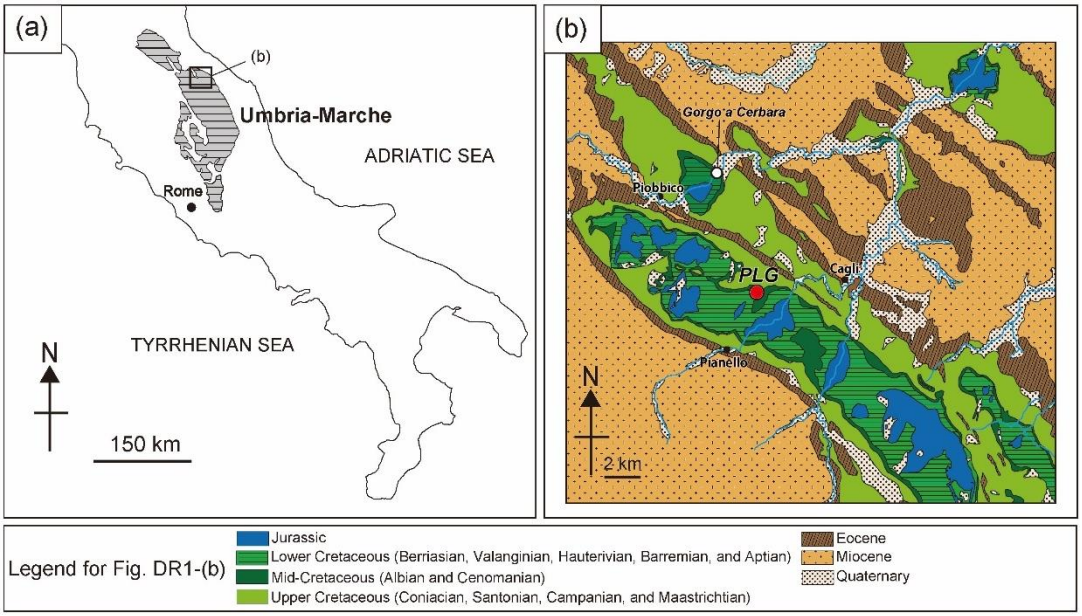

Fig. DR1: Geological map of Poggio le Guaine (PLG) revised from Matsumoto et al. (2020). PLG section is located at lat. 43°32’29.06” N, long. 12°34’51.09” E and the drilling site of the PLG core is located at lat. 43°32'42.72" N; long. 12°32'40.92" E. The location of the Gorgo a Cerbara section is also shown.

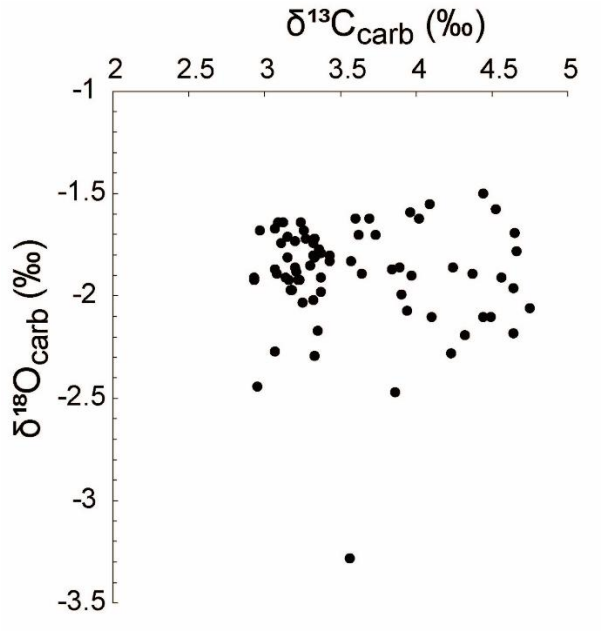

Fig. DR2: Cross plot of $\delta^{13}C_{carb}$ and $\delta^{18}O_{carb}$ of sedimentary rock samples of the Poggio le Guaine core.

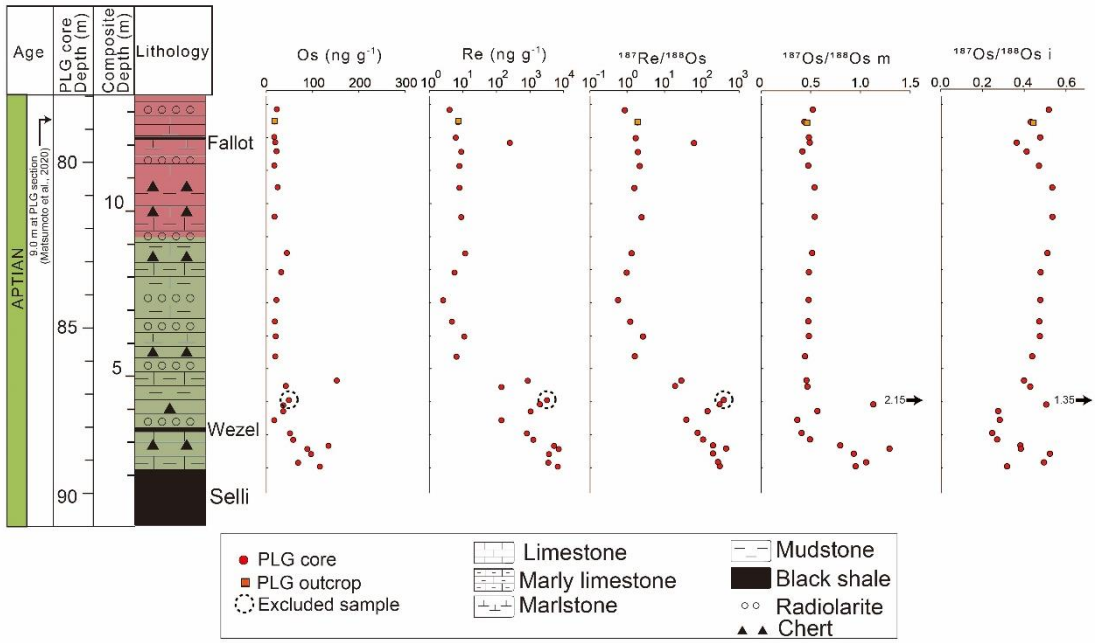

Fig. DR3: Os and Re data of sedimentary rock samples of PLG record.

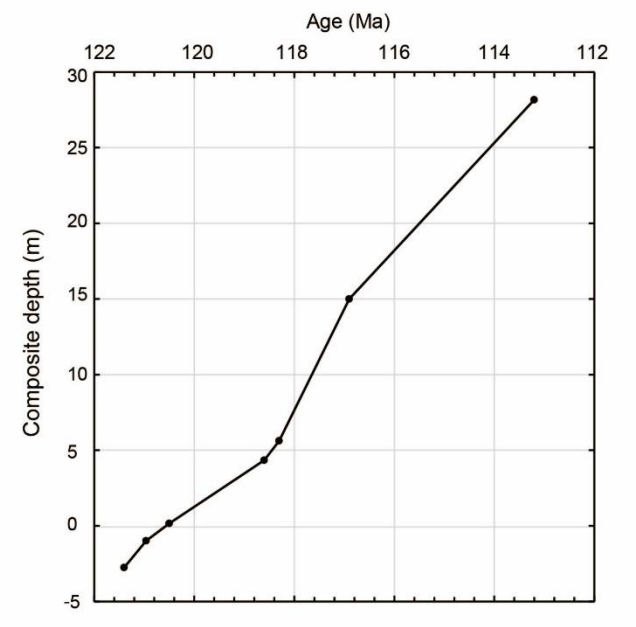

Fig. DR4: Age-depth model based on Table DR3

TABLE DR1. CARBONATE CARBON AND OXYGEN ISOTOPIC RATIO OF SEDIMENTARY ROCK SAMPLES OF PLG CORE

Sample Name	Lithology	δ^{13}C-PDB (‰)	δ^{18}O-PDB (‰)	δ^{13}C-1SD (‰)	δ^{18}O-1SD (‰)	Depth (Core) (m)	Depth (Composit) (m)
PLG-C 90.98	Marlstone	4.65	-1.69	0.09	0.05	89.20	2.34
PLG-C 90.85	Marlstone	4.23	-2.28	0.06	0.05	89.08	2.46
PLG-C 90.58	Mudstone	4.37	-1.89	0.06	0.05	88.82	2.72
PLG-C 90.42	Marlstone	4.44	-2.1	0.06	0.05	88.67	2.87
PLG-C 90.32	Mudstone	4.75	-2.06	0.06	0.05	88.57	2.97
PLG-C 90.13	Marlstone	4.24	-1.86	0.06	0.05	88.39	3.15
PLG-C 89.93	Marlstone	4.32	-2.19	0.06	0.05	88.19	3.35
PLG-C 89.53	Marlstone	3.94	-2.07	0.06	0.05	87.80	3.74
PLG-C 89.26	Marlstone	4.66	-1.78	0.06	0.05	87.53	4.01
PLG-C 89.06	Marlstone	4.1	-2.1	0.06	0.05	87.33	4.21
PLG-C 88.92	Marlstone	4.49	-2.1	0.06	0.05	87.19	4.35
PLG-C 88.52	Marlstone	4.64	-1.96	0.06	0.05	86.79	4.75
PLG-C 88.33	Mudstone	4.64	-2.18	0.06	0.05	86.60	4.94
PLG-C 87.99	Marlstone	4.53	-1.57	0.07	0.07	86.26	5.28
PLG-C 87.79	Marlstone	4.44	-1.5	0.08	0.05	86.06	5.48
PLG-C 87.67	Marlstone	4.56	-1.91	0.08	0.05	85.94	5.60
PLG-C 87.60	Mudstone	3.96	-1.59	0.08	0.05	85.87	5.67
PLG-C 87.41	Marlstone	3.9	-1.99	0.08	0.05	85.68	5.86
PLG-C 87.17	Marlstone	3.86	-2.47	0.08	0.05	85.44	6.10
PLG-C 87.03	Marlstone	4.09	-1.55	0.08	0.05	85.30	6.24
PLG-C 86.99	Marlstone	4.02	-1.62	0.08	0.05	85.26	6.28
PLG-C 86.92	Mudstone	3.97	-1.9	0.08	0.05	85.19	6.35
PLG-C 86.84	Marlstone	3.84	-1.87	0.08	0.05	85.11	6.43
PLG-C 86.79	Mudstone	3.89	-1.86	0.08	0.05	85.06	6.48
PLG-C 86.68	Marlstone	3.6	-1.62	0.08	0.05	84.95	6.59
PLG-C 86.54	Marlstone	3.57	-1.83	0.06	0.05	84.81	6.73
PLG-C 86.44	Marlstone	3.64	-1.89	0.06	0.05	84.71	6.83
PLG-C 86.38	Mudstone	3.43	-1.83	0.06	0.05	84.65	6.89
PLG-C 86.17	Marlstone	3.56	-3.28	0.06	0.05	84.44	7.10
PLG-C 86.01	Marlstone	3.62	-1.7	0.06	0.05	84.28	7.26
PLG-C 85.94	Mudstone	3.69	-1.62	0.06	0.05	84.21	7.33
PLG-C 85.89	Marlstone	3.73	-1.7	0.06	0.05	84.16	7.38
PLG-C 85.77	Mudstone	3.37	-1.79	0.06	0.05	84.04	7.50
PLG-C 85.48	Marlstone	3.43	-1.8	0.06	0.05	83.75	7.79
PLG-C 85.05	Mudstone	3.33	-2.29	0.06	0.05	83.32	8.22
PLG-C 84.90	Marlstone	3.37	-1.91	0.06	0.05	83.17	8.37
PLG-C 84.78	Marlstone	3.33	-1.72	0.08	0.05	83.05	8.49
PLG-C 84.70	Mudstone	3.36	-1.77	0.08	0.05	82.97	8.57
PLG-C 84.51	Marlstone	3.35	-2.17	0.08	0.05	82.78	8.76
PLG-C 84.40	Mudstone	2.95	-2.44	0.08	0.05	82.67	8.87
PLG-C 84.36	Mudstone	2.93	-1.92	0.08	0.05	82.63	8.91
PLG-C 84.27	Marlstone	3.23	-1.92	0.08	0.05	82.54	9.00
PLG-C 84.08	Marlstone	3.32	-2.02	0.08	0.05	82.35	9.19
PLG-C 83.92	Mudstone	2.93	-1.91	0.08	0.05	82.19	9.35
PLG-C 83.67	Marlstone	3.17	-1.97	0.08	0.05	81.94	9.60
PLG-C 83.47	Mudstone	3.37	-1.98	0.08	0.05	81.74	9.80
PLG-C 83.37	Marlstone	3.12	-1.64	0.08	0.05	81.64	9.90
PLG-C 83.05	Mudstone	3.33	-1.81	0.06	0.05	81.32	10.22
PLG-C 82.86	Mudstone	3.32	-1.74	0.06	0.05	81.13	10.41
PLG-C 82.73	Marlstone	3.27	-1.72	0.06	0.05	81.00	10.54
PLG-C 82.61	Marlstone	3.32	-1.8	0.06	0.05	80.88	10.66
PLG-C 82.48	Marlstone	3.26	-1.68	0.06	0.05	80.75	10.79
PLG-C 82.32	Marlstone	3.3	-1.85	0.06	0.05	80.59	10.95
PLG-C 82.15	Mudstone	3.25	-2.03	0.06	0.05	80.44	11.10
PLG-C 82.01	Mudstone	3.07	-2.27	0.06	0.05	80.28	11.26
PLG-C 81.91	Mudstone	2.97	-1.68	0.06	0.05	80.18	11.36
PLG-C 81.82	Mudstone	3.09	-1.64	0.06	0.05	80.09	11.45
PLG-C 81.61	Marlstone	3.2	-1.86	0.06	0.05	79.88	11.66
PLG-C 81.56	Marlstone	3.22	-1.92	0.06	0.05	79.83	11.71
PLG-C 81.47	Marlstone	3.18	-1.97	0.08	0.05	79.74	11.80
PLG-C 81.35	Marlstone	3.07	-1.87	0.08	0.05	79.66	11.88
PLG-C 81.23	Marlstone	3.08	-1.89	0.08	0.05	79.50	12.04
PLG-C 81.12	Marlstone	3.14	-1.91	0.08	0.05	79.39	12.15
PLG-C 80.96	Marlstone	3.15	-1.81	0.08	0.05	79.23	12.31
PLG-C 80.92	Marlstone	3.21	-1.88	0.08	0.05	79.19	12.35
PLG-C 80.71	Marlstone	3.15	-1.71	0.08	0.05	78.98	12.56
PLG-C 80.67	Marlstone	3.24	-1.64	0.08	0.05	78.94	12.60
PLG-C 80.49	Marlstone	3.2	-1.73	0.08	0.05	78.76	12.78
PLG-C 80.35	Marlstone	3.16	-1.92	0.08	0.05	78.62	12.92
PLG-C 80.23	Marlstone	3.07	-1.67	0.08	0.05	78.50	13.04
PLG-C 80.12	Marlstone	3.11	-1.74	0.08	0.05	78.39	13.15

TABLE DR2. Os AND Re DATA OF SEDIMENTARY ROCK SAMPLES OF PLG RECORD.

Sample Name	Lithology	Os	1SD	$^{187}Os/^{188}Os$ m	1SD	Re	1SD	$^{187}Re/^{188}Os$	1SD	Osi	1SD	Age	Depth(core)	Depth(composit)	Comments
		(pg g^{-1})				(pg g^{-1})						(Ma)	(m)	(m)	
PLG core															
PLG-C 90.98	Marlstone	116.8	0.5	0.952	0.007	6.74.E+03	6.E+01	308	3	0.337	0.009	119.8	89.20	2.3	
PLG-C 90.85	Marlstone	69.5	0.4	1.058	0.010	3.52.E+03	9.E+01	274	7	0.512	0.019	119.8	89.08	2.5	
PLG-C 90.58	Mudstone	97.6	0.4	0.933	0.006	3.66.E+03	1.8.E+02	199	9.9	0.535	0.02	119.6	88.82	2.7	
PLG-C 90.42	Marlstone	89.6	0.6	1.295	0.013	7.14.E+03	1.7.E+02	442	11	0.413	0.03	119.6	88.67	2.9	
PLG-C 90.32	Mudstone	135.2	0.9	0.796	0.011	5.21.E+03	9.E+01	202	4	0.394	0.013	119.5	88.57	3.0	
PLG-C 90.13	Mudstone	59.1	0.4	0.490	0.007	1.257.E+03	1.8.E+01	107	2	0.276	0.008	119.4	88.39	3.2	
PLG-C 89.93	Marlstone	52.1	0.3	0.404	0.007	8.06.E+02	1.3.E+01	77.2	1.3	0.251	0.007	119.3	88.19	3.3	Just below Wezel Level
PLG-C 89.53	Marlstone	18.0	0.2	0.361	0.013	1.41.E+02	3.E+00	38.7	1.1	0.284	0.013	119.1	87.80	3.7	Just above Wezel Level
PLG-C 89.26	Marlstone	37.6	0.18	0.565	0.006	1.045.E+03	1.6.E+01	142	2	0.284	0.008	119.0	87.53	4.0	
PLG-C 89.06	Marlstone	36.5	0.30	1.131	0.019	2.046.E+03	1.9.E+01	305	4	0.504	0.02	118.9	87.33	4.2	
PLG-C 88.92	Marlstone	49.6	0.19	2.156	0.013	3.20.E+03	1.7.E+02	393	21	1.377	0.05	118.8	87.19	4.4	Excluded
PGL-C 88.52	Marlstone	43.1	0.39	0.464	0.010	1.54.E+02	1.0.E+01	17.9	1.2	0.427	0.011	118.5	86.79	4.8	
PLG-C 88.33	Mudstone	153.4	0.7	0.454	0.003	8.53.E+02	1.1.E+01	27.9	0.4	0.399	0.003	118.3	86.60	4.9	
PLG-C 87.60	Mudstone	20.4	0.2	0.440	0.011	6.E+00	1.0.E+01	2	3	0.437	0.012	117.7	85.87	5.7	
PLG-C 86.99	Marlstone	21.2	0.14	0.479	0.007	1.1.E+01	8.E+00	2.6	1.8	0.474	0.008	117.6	85.26	6.3	
PLG-C 86.54	Marlstone	19.5	0.18	0.473	0.009	4.7.E+00	1.1.E+00	1.2	0.3	0.471	0.009	117.5	84.81	6.7	
PLG-C 85.89	Marlstone	22.8	0.14	0.476	0.007	3.E+00	5.E+00	0.6	1.0	0.475	0.007	117.4	84.16	7.4	
PLG-C 85.05	Mudstone	35.0	0.3	0.477	0.013	6.E+00	2.E+00	0.9	0.3	0.475	0.010	117.2	83.32	8.2	
PLG-C 84.47	Mudstone	45.5	0.2	0.512	0.005	1.17.E+01	1.0.E+00	1.30	0.11	0.509	0.005	117.1	82.74	8.8	
PLG-C 83.37	Marlstone	18.6	0.1	0.538	0.007	8.9.E+00	1.0.E+00	2.4	0.3	0.533	0.007	116.9	81.64	9.9	
PLG-C 82.48	Marlstone	25.4	0.2	0.536	0.009	8.E+00	9.E+00	1.6	1.8	0.533	0.010	116.7	80.75	10.8	
PLG-C 81.82	Marlstone	18.3	0.10	0.473	0.007	7.8.E+00	1.0.E+00	2.2	0.3	0.469	0.007	116.6	80.09	11.4	
PLG-C 81.35	Marlstone	23.1	0.14	0.414	0.006	9.E+00	6.E+00	1.9	1.3	0.410	0.007	116.5	79.66	11.9	
PLG-C 81.12	Marlstone	20.3	0.12	0.487	0.007	2.50.E+02	5.E+00	62.1	1.4	0.366	0.008	116.4	79.39	12.1	Just below Fallot Level
PLG-C 80.96	Marlstone	18.1	0.10	0.478	0.007	6.1.E+00	1.2.E+00	1.7	0.3	0.475	0.007	116.4	79.23	12.3	Just above Fallot Level
PLG-C 80.49	Marlstone	18.9	0.14	0.433	0.008	7.1.E+00	1.3.E+00	1.9	0.4	0.430	0.008	116.3	78.76	12.8	
PLG-C 80.12	Marlstone	23.6	0.2	0.518	0.015	4.E+00	6.E+00	0.9	1.2	0.516	0.015	116.2	78.39	13.1	
PLG section													Depth (outcrop)		
PLG-9	Marlstone	22	0.16	0.448	0.009	7.8.E+00	1.3.E+00	1.8	0.29	0.445	0.009	116.3	9 m	12.5	

TABLE DR3. AGE MODEL

Horizons	Age (Ma)	Depth (m)
LO *M. renilaevis*	113.2	28.2
HO *G. algerianus*	116.9	15.0
LO *G. algerianus*	118.3	5.6
HO *L. cabri*	118.6	4.4
LO *L. cabri*	120.5	0.2
Top of CM0r	121.0	-1.0
Base of CM0r	121.4	-2.8

Note1. G.=Globigerinelloides, L.=Leupoldina, P.=Paraticinella, M.=Microhedbergella,

Note2. Age is based on Gale et al. (2020)

Note3. Depth is based on Coccioni (2020), and Matsumoto et al. (2020).

REFERENCE

Allègre, C. J., and Luck, J. M., 1980, Os isotopes as petrogenetic and geological tracers: Earth and Planetary Science Letters, v. 48, p. 148–154, doi: 10.1016/0012-821X(80)90177-6.

Aguado, R., de Gea, G. A., Castro, J. M., O'Dogherty, L., Quijano, M. L., Naafs, B. D. A., and Pancost, R. D., 2014, Late Barremian–early Aptian dark facies of the Subbetic (Betic Cordillera, southern Spain): Calcareous nannofossil quantitative analyses, chemostratigraphy and palaeoceanographic reconstructions: Palaeogeography, Palaeoclimatology, Palaeoecology, v. 395, p. 198–221, doi: 10.1016/j.palaeo.2013.12.031.

Blättler, C. L., Jenkyns, H. C., Reynard, L. M., and Henderson, G. M., 2011, Significant increases in global weathering during Oceanic Anoxic Events 1a and 2 indicated by calcium isotopes: Earth and Planetary Science Letters, v. 309, p. 77–88, doi: 10.1016/j.epsl.2011.06.029.

Coccioni, R., 2020, Revised upper Barremian–upper Aptian planktonic foraminiferal biostratigraphy of the Gorgo a Cerbara section (central Italy): Newsletters on Stratigraphy, v. 53, p. 275–295, doi: 10.1127/nos/2019/0539.

Coccioni, R., Nesci, O., Tramontana, M., Wezel, F. C., and Moretti, E., 1987, Descrizione di un livello–guida “radiolaritico–bituminoso–ittiolitico” alla base delle Marne a

169 Fucoidi nell'Appennino Umbro–Marchigiano. Bollettino della Società Geologica
170 Italiana v. 106, p. 183–192.
171 Coccioni, R., Jovane, L., Bancalà, G., Bucci, C., Fauth, G., Frontalini, F., Janikian, L.,
172 Savian, J., Paes de Almeida, R., Mathias, G. L., and Ferreira da Trindade, R. I., 2012,
173 Umbria-Marche Basin, Central Italy: A reference section for the Aptian-Albian
174 interval at low latitudes: Scientific Drilling, v. 13, p. 42–46, doi:
175 10.2204/iodp.sd.13.07.2011.
176 Coccioni, R., Sabatino, N., Frontalini, F., Gardin, S., Sideri, M., Sprovieri, M., 2014, The
177 negleted history of Oceanic Anoxic Event 1b: insights and new data from the Poggio
178 le Guaine section (Umbria–Marche Basin): Stratigraphy, v. 11, p. 245–282.
179 De Gea, G. A., Castro, J. M., Aguado, R., Ruiz-Ortiz, P. A., and Company, M., 2003,
180 Lower Aptian carbon isotope stratigraphy from a distal carbonate shelf setting: the
181 Cau section, Prebetic zone, SE Spain: Palaeogeography, Palaeoclimatology,
182 Palaeoecology, v. 200, p. 207-219, doi: 10.1016/S0031-0182(03)00451-6.
183 Elkhazri, A., Abdallah, H., Razgallah, S., Moullade, M., and Kuhnt, W., 2013, Carbon-
184 isotope and microfaunal stratigraphy bounding the Lower Aptian Oceanic Anoxic
185 Event 1a in northeastern Tunisia: Cretaceous Research, v. 39, p. 133–148, doi:
186 10.1016/j.cretres.2012.05.011.

187 Erba, E., Channell, J. E., Claps, M., Jones, C., Larson, R., Opdyke, B., Silva, I., P., Riva,
188 A., Salvini, G., and Torricelli, S., 1999). Integrated stratigraphy of the Cismon
189 Apticore (southern Alps, Italy); a" reference section" for the Barremian-Aptian
190 interval at low latitudes. *The Journal of Foraminiferal Research*, *29*(4), 371–391.
191 Heimhofer, U., Hochuli, P. A., Herrle, J. O., and Weissert, H., 2006, Contrasting origins
192 of Early Cretaceous black shales in the Vocontian basin: Evidence from palynological
193 and calcareous nannofossil records: Palaeogeography, Palaeoclimatology,
194 Palaeoecology, v. 235, p. 93–109, doi: 10.1016/j.palaeo.2005.09.025.
195 Herrle, J. O., Kößler, P., Friedrich, O., Erlenkeuser, H., and Hemleben, C., 2004, High-
196 resolution carbon isotope records of the Aptian to Lower Albian from SE France and
197 the Mazagan Plateau (DSDP Site 545): a stratigraphic tool for paleoceanographic and
198 paleobiologic reconstruction: Earth and Planetary Science Letters, v. 218, p. 149–161,
199 doi: 10.1016/S0012-821X(03)00646-0.
200 Hu, X., Zhao, K., Yilmaz, I. O., and Li, Y., 2012, Stratigraphic transition and
201 palaeoenvironmental changes from the Aptian oceanic anoxic event 1a (OAE1a) to
202 the oceanic red bed 1 (ORB1) in the Yenicesihlar section, central Turkey: Cretaceous
203 Research, v. 38, p. 40–51, doi: 10.1016/j.cretres.2012.01.007.
204 Kößler, P., Herrle, J. O., Appel, E., Erbacher, J., and Hemleben, C., 2001, Magnetic

records of climatic cycles from mid-Cretaceous hemipelagic sediments of the Vocontian Basin, SE France: Cretaceous Research, v. 22, p. 321–331, doi: 10.1006/cres.2001.0256.

Levasseur, S., Birck, J. L., and Allègre, C. J., 1998, Direct measurement of femtomoles of osmium and the $^{187}Os/^{186}Os$ ratio in seawater: Science, v. 282, p. 272–274.

Levasseur, S., Birck, J. L., and Allegre, C. J., 1999, The osmium riverine flux and the oceanic mass balance of osmium: Earth and Planetary Science Letters, v. 174, p. 7–23, doi: 10.1016/S0012-821X(99)00259-9.

Luciani, V., Cobianchi, M., and Jenkyns, H. C., 2001, Biotic and geochemical response to anoxic events: the Aptian pelagic succession of the Gargano Promontory (southern Italy): Geological Magazine, v. 138, p. 277–298.

Malinverno, A., Hildebrandt, J., Tominaga, M., and Channell, J. E., 2012, M-sequence geomagnetic polarity time scale (MHTC12) that steadies global spreading rates and incorporates astrochronology constraints: Journal of Geophysical Research: Solid Earth, v. 117(B6), doi 10.1029/2012JB009260.

Matsumoto, H., Kuroda, J., Coccioni, R., Frontalini, F., Sakai, S., Ogawa, N. O., and Ohkouchi, N., 2020, Marine Os isotopic evidence for multiple volcanic episodes during Cretaceous Oceanic Anoxic Event 1b: Scientific Reports, v. 10, 12601, doi:

10.1038/s41598-020-69505-x.

Palmer, M. R., and Edmond, J. M., 1989, The strontium isotope budget of the modern ocean: Earth and Planetary Science Letters, v. 92, p. 11–26, doi: 10.1016/0012-821X(89)90017-4.

Peucker-Ehrenbrink, B., and Jahn, B. M., 2001, Rhenium-osmium isotope systematics and platinum group element concentrations: Loess and the upper continental crust: Geochemistry, Geophysics, Geosystems, v. 2, p. 1061, doi: 10.1029/2001GC000172.

Quijano, M. L., Castro, J. M., Pancost, R. D., de Gea, G. A., Najarro, M., Aguado, R., Rosales, I., and Martín-Chivelet, J., 2012, Organic geochemistry, stable isotopes, and facies analysis of the Early Aptian OAE—New records from Spain (Western Tethys): Palaeogeography, Palaeoclimatology, Palaeoecology, v. 365, p. 276–293, doi: 10.1016/j.palaeo.2012.09.033.

Savian, J., Trindade, R., Janikian, L., Jovane, L., de Almeida, R. P., Coccioni, R., Frontalini, F., Sideri, M., and Jenkyns, H. C. (2016). The Barremian-Aptian boundary in the Poggio le Guaine core (central Italy): Evidence for magnetic polarity Chron M0r and oceanic anoxic event 1a. *in* Menichetti, M., Coccioni, R., and Montanari, A., eds., The Stratigraphic Record of Gubbio: Integrated Stratigraphy of the Late

241 Cretaceous–Paleogene Umbria-Marche Pelagic Basin: The Geological Society of
242 America Special Paper, 524, p. 57–78, doi:10.1130/2016.2524(05).
243 Shirai, K., Koyama, F., Murakami-Sugihara, N., Nanjo, K., Higuchi, T., Kohno, H.,
244 Watanabe, Y., Okamoto, K., and Sano, M., 2018, Reconstruction of the salinity
245 history associated with movements of mangrove fishes using otolith oxygen isotopic
246 analysis: Marine Ecology Progress Series, v. 593, p. 127–139, doi:
247 10.3354/meps12514.
248 Smoliar, M. I., Walker, R. J., and Morgan, J. W., 1996, Re-Os ages of group IIA, IIIA,
249 IVA, and IVB iron meteorites: Science, v. 271, p. 1099–1102, doi:
250 10.1126/science.271.5252.1099.
251 Tejada, M. L. G., Suzuki, K., Kuroda, J., Coccioni, R., Mahoney, J. J., Ohkouchi, N.,
252 Sakamoto, T. and Tatsumi, Y., 2009, Ontong Java Plateau eruption as a trigger for the
253 early Aptian oceanic anoxic event: Geology, v. 37, p. 855–858, doi:
254 10.1130/G25763A.1.
255 Tornaghi, M. E., Silva, I. P., and Ripepe, Maurizio, 1989, Lithostratigraphy and
256 planktonic foraminiferal biostratigraphy of the Aptian-Albian" Scisti a Fucoidi" in
257 the Piobbico core, Marche, Italy: background for cyclostratigraphy: Rivista Italiana
258 di Paleontologia e Stratigrafia, v. 95, p. 223–264.